SPECT/CT Imaging of Pluronic Nanocarriers with Varying Poly(ethylene oxide) Block Length and Aggregation State

Arranja, Alexandra; Ivashchenko, Oleksandra; Denkova, Antonia G.; Morawska, Karolina; Van Vlierberghe, Sandra; Dubruel, Peter; Waton, Gilles; Beekman, Freek J.; Schosseler, François; Mendes, Eduardo

DOI
10.1021/acs.molpharmaceut.5b00958

Publication date
2016

Document Version
Accepted author manuscript

Published in
Molecular Pharmaceutics

SPECT/CT imaging of Pluronic nanocarriers with varying PEO block length and aggregation state

Journal:	*Molecular Pharmaceutics*
Manuscript ID	mp-2015-009586
Manuscript Type:	Article
Date Submitted by the Author:	18-Dec-2015

Complete List of Authors:	Arranja, Alexandra; Institut Charles Sadron, Ivashchenko, Oleksandra; Delft University of Technology, Radiation Science and Technology Denkova, Antonia; Delft University of Technology, Morawska, Karolina; Ghent University, Organic and Macromolecular Chemistry Van Vlierberghe, Sandra; University of Gent, Polymer Chemistry and Biomaterials Research Group Waton, Gilles; Université de Strasbourg , Institut Charles Sadron (CNRS) Dubruel, Peter; Ghent University, Polymer Chemistry & Biomaterials Research Group Beekman, Freek; Delft University of Technology, Radiation Science and Technology Schosseler, François; Institut Charles Sadron, Mendes, Eduardo; Delft University of Technology, Section Advanced Soft Matter(ASM)

SPECT/CT imaging of Pluronic nanocarriers with varying PEO block length and aggregation state

Alexandra Arranja[¶,†,‡,*], *Oleksandra Ivashchenko*[¶,‡,§,⊥,*], *Antonia G. Denkova*[‡], *Karolina Morawska*[‖], *Sandra van Vlierberghe*[‖], *Peter Dubruel*[‖], *Gilles Waton*[†], *Freek J. Beekman*[‡,§,⊥], *François Schosseler*[†] *and Eduardo Mendes*[▽]

[†] Institut Charles Sadron (CNRS), Strasbourg, France

[‡] Department of Radiation Science and Technology, Delft University of Technology, Delft, The Netherlands

[§] MILabs B.V., Utrecht, The Netherlands

[⊥] Department of Translational Neuroscience, Brain Center Rudolf Magnus, University Medical Center, Utrecht, The Netherlands

[‖] Department of Organic and Macromolecular Chemistry, Ghent University, Ghent, Belgium

[▽] Department of Chemical Engineering, Delft University of Technology, Delft, The Netherlands

[¶] These authors contributed equally to the work.

***Corresponding authors**

Oleksandra Ivashchenko, Reactor Institute Delft, Section Radiation, Detection & Medical Imaging, Mekelweg 15, 2629 JB, Delft, The Netherlands. Tel: +31(0)621396112. Email: O.Ivashchenko-1@tudelft.nl

Dr. Alexandra Arranja, Advanced Soft Matter, Department of Chemical Engineering, Delft University of Technology, Julianalaan 136, 2628BL Delft, The Netherlands. Tel: +31(0)15 278 9418. Email: A.GilArranja-1@tudelft.nl

TABLE OF CONTENTS/ ABSTRACT GRAPHIC

ABSTRACT

Optimal biodistribution and prolonged circulation of nanocarriers improves diagnostic and therapeutic effects of EPR-based nanomedicines. Despite extensive use of Pluronics in polymer-based pharmaceuticals, the influence of different PEO block length and aggregation state on the biodistribution of the carriers is rather unexplored. In this work, we studied these effects by evaluating the biodistribution of Pluronic unimers and cross-linked micelles with different PEO block size. *In vivo* biodistribution of ^{111}In-radiolabeled Pluronic nanocarriers was performed in healthy mice using SPECT/CT.

All carriers show fast uptake in the organs from the reticuloendothelial system followed by a steady elimination through the hepatobiliary tract and renal filtration. The PEO block length affects the initial renal clearance of the compounds and the overall liver uptake. The aggregation state influences the long-term accumulation of the nanocarriers in the liver.

We showed that the circulation time and elimination pathways can be tuned by varying the physicochemical properties of Pluronic copolymers. Our results can be beneficial for the design of future Pluronic-based nanomedicines.

Keywords: Pluronic, unimers, micelles, SPECT

INTRODUCTION

Nanocarriers including polymers, micelles and nanoparticles, have a number of advantages over low molecular weight agents.[1] Application of these carriers is particularly interesting in oncology, where the leaky vasculature of tumors and the impaired lymphatic drainage allows to reach high drug accumulation and retention via the well-known Enhanced Permeability and Retention (EPR) effect.[2] This effect strongly depends on the blood circulation time and biodistribution of the nanocarriers, parameters that are mostly determined by their physicochemical properties such as size, shape and surface charge.[3]

The development of polymer-based nanocarriers is particularly powerful since they can be easily tailored with appropriate functionalization and/or size to meet the set requirements and more efficiently deliver their cargo to diseased sites. The polymer selection criteria for clinical applications includes controlled stability, biocompatibility, aqueous solubility and availability to attach chemical groups that can be used for targeting, imaging or therapy.[4] Among the several polymers used for the development of polymer-based nanocarriers, Pluronics are probably the most broadly investigated. Pluronics are amphiphilic triblock copolymers composed of PEO-PPO-PEO, where PEO stands for poly(ethylene oxide) and PPO denotes poly(propylene oxide). Due to their amphiphilic properties, Pluronic unimers can aggregate and self-assemble into micelles composed by a hydrophilic hydrated PEO corona and hydrophobic PPO core, which can be used to incorporate hydrophobic drugs. This self-assembling mechanism depends mainly on the solution temperature and composition (e.g. salts and proteins) as well as on the polymer concentration, resulting in micelle formation above a critical micelle temperature (cmT) and/or polymer concentration (cmc). Therefore, Pluronic micelles have a dynamic nature which may result in their rapid disintegration upon dilution in the bloodstream,[5, 6] ultimately affecting their biodistribution.

Despite the broad use of Pluronics in pharmaceutical formulations, very few groups studied the effects influencing the *in vivo* biodistribution of Pluronic copolymers.[7-10] Only one studied the effect of the aggregation state using different polymer doses,[9] whereas the effect of the PEO block length and aggregation state using similar concentrations has not yet been reported.

In this work, we developed a new strategy to compare the biodistribution of molecular and core-stabilized supramolecular nanocarriers based on Pluronic copolymers. This approach eliminates the limitation associated with the dynamic nature of copolymer micelles and allows using similar concentrations of both nanocarriers, resulting in more meaningful comparison of their biodistribution. We used Single Photon Emission Computed Tomography (SPECT) and performed longitudinal biodistribution studies of ^{111}In-labeled Pluronic nanocarriers (unimers and stabilized micelles). Two Pluronics (P94 and F127) with similar PPO block lengths and different PEO block masses (≈1100 and 4250 g/mol) were used. In addition, the early biokinetics of the most frequently applied Pluronic (F127) was investigated.

EXPERIMENTAL SECTION

Functionalization of Pluronic copolymers with DTPA

Pluronic block copolymers (P94 and F127, BASF) were purified from low molecular weight contaminants. They were modified with 1,1-carbodiimidazole (CDI-Pluronic) followed by primary amines (Pluronic-NH_2) using a procedure similar to the one in Lu *et al.* for Pluronic F68.[11] The modified chelator *p*-SCN-Bn-DTPA was conjugated to the amine terminated copolymers using a procedure previously reported for the diblock PEG-PCL.[12] Briefly, *p*-SCN-Bn-DTPA dissolved in DMSO (50 mg/ml) was added in a 1:1 molar ratio of reacting groups to a 25 mg/ml solution of the copolymers F127-NH_2 or P94-NH_2 in sodium

bicarbonate buffer (0.1 M, pH 8.5). The solutions were stirred at room temperature for at least 4 h. Characterization of the raw, CDI-activated and amine modified copolymers was performed by ^{1}H-NMR (Bruker WH 300 MHz instrument) after reaction with trichloroacetyl isocyanate at room temperature in deuterated chloroform, and analyzed in their powder form by FT-IR in a PerkinElmer Frontier FT-IR (midIR) combined with a MKII Golden Gate set-up equipped with a diamond crystal from Specac.

Polymers conjugation efficiency

The conjugation efficiency of *p*-SCN-Bn-DTPA was determined by thin layer chromatography (TLC) of radiolabeled copolymers. The nanocarriers F127-DTPA and P94-DTPA diluted in PBS were labelled with 1 MBq of $^{111}InCl_3$ and incubated for 30 min at room temperature. The TLC was performed in Aluminum sheets of silica gel 60 using a sodium acetate buffer (0.1 M, pH 5.8) as the eluent. Purification from unreacted *p*-SCN-Bn-DTPA was performed by size exclusion chromatography (SEC) using prepacked Sephadex G25 columns and MilliQ water as the eluent.

Preparation of stabilized Pluronic F127 and P94 micelles with DTPA

Stabilized polymeric micelles (SPM) were prepared from a mixture of 10% F127-DTPA or 3.65% P94-DTPA functionalized copolymers with regular copolymers in aqueous solution at a total copolymer concentration of 2.5% w/w. The self-assembled Pluronic micelles were then cross-linked as previously described[5] to obtain stabilized micelles with the chelator DTPA in their corona (SPM-F127-DTPA and SPM-P94-DTPA). Free remaining unimers and free *p*-SCN-Bn-DTPA were removed, respectively, by diafiltration at 5^{o}C (Amicon Ultra-4 30K) and by SEC (Sephadex G25 columns).

Physicochemical characterization

The average size of Pluronic unimers and cross-linked micelles was determined by dynamic light scattering (DLS). The hydrodynamic diameters (D_H) were calculated from the decay times using the Stokes-Einstein equation. The superficial charge of the stabilized micelles was measured through zeta potential (mV) determination (Zetasizer Nano ZS, Malvern Instruments, UK).

Radiolabeling of Pluronic nanocarriers with ^{111}In and purification

F127-DTPA, SPM-F127-DTPA, P94-DTPA and SPM-P94-DTPA were prepared in 1X PBS buffer and 75 MBq of $^{111}InCl_3$ were added to each sample at room temperature and incubated for 30 minutes. Radiochemical purity was evaluated by TLC using EDTA:NH_4Ac (1:1) (v:v) (0.1 M, pH 5.5).

Samples with labelling efficiency higher than 95% were used without further purification. Samples with a lower coupling efficiency were further purified by addition of free DTPA to the labelling mixtures and by subsequent elution through a prepacked Sephadex G25 column using 1X PBS as the eluent. The purification efficiency for the eluted fractions was then evaluated by TLC.

In vitro radiostability in mouse serum and PBS

Radiostability of F127-DTPA-^{111}In, P94-DTPA-^{111}In, SPM-F127-DTPA-^{111}In and SPM-P94-DTPA-^{111}In was measured *in vitro* by incubation of 50µL of radiolabeled samples with 350µL of PBS or mouse serum at 37^{o}C for 72 h. At various time points, 5 µL aliquots of the solutions were spotted in the bottom of TLC strips and developed in the EDTA:NH_4Ac (1:1) (v:v) (0.1 M, pH 5.5) eluent to evaluate the dissociation of ^{111}In from the samples. In this system, it is possible to assess transchelation to serum proteins as R_f Pluronic-DTPA-^{111}In=0.0, R_f

Proteins-^{111}In=0.5 and R_f free ^{111}In=1.0. Free ^{111}In and *p*-SCN-Bn-DTPA-^{111}In were used as controls.

Animal handling

Animal experiments were performed with A/J mice according to protocols approved by the Animal Ethical Committee of the UMC Utrecht and in accordance with Dutch Law on Animal experimentation.

Eight mice were divided into four study groups and assigned for imaging with F127-DTPA-^{111}In, SPM-F127-DTPA-^{111}In, P94-DTPA-^{111}In and SPM-P94-DTPA-^{111}In. All animals were anesthetized with isoflurane and injected with the radioactive compounds in the tail vein. Average injected activities were 3.6 MBq and 0.014 g/kg of compound.

Total body SPECT/CT scans of 30 minutes were acquired at 0 (immediately after injection), 24 and 48 hours post-injection (p.i.). After the end of the 48 hours p.i. total body scans, an additional 30 min scan was performed focusing on the abdominal area to acquire information on late-stage biodistribution in the spleen and liver.

To evaluate early stage dynamics of F127-DTPA-^{111}In, one mouse from the F127-DTPA-^{111}In study group was anesthetized and a tail vein catheter was applied. The animal was injected with the compound just after the start of the dynamic total body SPECT acquisition with 15-second frames.

SPECT/CT imaging and data analyzing

Animals were imaged in U-SPECT^{+}/CT scanner (MILabs, the Netherlands). This system is equipped with a three stationary scintillator detectors that are arranged in triangular setup and an integrated X-ray micro-CT scanner.

The SPECT scans were acquired in list-mode data format with use of 2.0 mm mouse pinhole collimator.[13] After this, SPECT image reconstructions were carried out with a pixel-based order-subset expectation maximization (POSEM)[14] algorithm that included resolution recovery and compensation for distance-dependent pinhole sensitivity.[15] All reconstructions were performed with use of 4 subsets, 12 iterations and an isotropic 0.4-mm-voxel grid. Triple-energy-window based Compton scatter correction according to King *et al.*[16] with 4% background windows and a 20% photo-peak energy window centered at 171 keV was performed. Effects of gamma-attenuation in the animal and bed were corrected for using CT data, after which absolute quantification of SPECT images was enabled using a scaling factor obtained from scanning a small ^{111}In source with known activity.[17]

For visual representation in the manuscript, reconstructed volumes were filtered with 1.2 mm full width at half maximum (FWHM) 3D Gaussian filter. Time-activity curves (TACs) derived from dynamic SPECT scan were generated from manually drawn region-of-interests (ROI), using decay-corrected but otherwise unprocessed images, reconstructed as a dynamic frame sequence.

To calculate the uptake of radiolabeled compound in the organs of interest, the registered to CT and quantitative 3D SPECT images were analyzed using PMOD 3.6 biomedical image analyzing software (PMOD, Zurich, Switzerland). A 3D region-of-interest (ROI) was manually drawn to encompass the radioactivity uptake in the organ. Separate ROI's were drawn for the radioactivity uptakes in the heart, liver, spleen, kidneys, brain and lungs. The uptake was expressed as % injected dose (%ID) per mL of tissue volume (%ID/mL).

All quantification data was reported as mean ± standard deviation within one study group. Correlations between the biodistribution of nanocarriers with different PEO block length and aggregation state were calculated using Pearson's correlation coefficient. All other statistic

comparisons were made using the Student's *t* test. MATLAB R2013b software was used for all statistic evaluations.

RESULTS

Synthesis of DTPA-functionalized Pluronic nanocarriers

Table 1 summarizes the characteristics of the employed Pluronics as determined by ^{1}H-NMR and TLC. While the PPO block has practically the same length in both copolymers, the PEO length is four times larger for the Pluronic F127. Pluronic unimers were first end-functionalized with the hydrophilic chelator DTPA according to the scheme available in the supplementary information (Scheme S1). In the ^{1}H-NMR spectrum of Pluronic-CDI (Figure 1), peaks from the imidazole moiety protons (δ=8.15 ppm, δ=7.44 ppm and δ=7.06 ppm) and from the ethylene oxide group adjacent to the imidazole carbonate group (δ=4.55 ppm) can be visualized. The protons of the -CH_2NH_2 methylene groups of the amine modified Pluronics were detected by the appearance of a triplet at δ=2.82 ppm. FT-IR analysis the copolymers and of the intermediate CDI-activated or amine-modified Pluronics are available in the supplementary information (Figure S1).

The modified chelator *p*-SCN-Bn-DTPA was conjugated to the amine terminated block copolymers (P94-NH_2 and F127-NH_2) by reaction of the primary amine with the reactive chelator isothiocyanate group to form a stable thiourea bond according to Figure S1. The corresponding functionalization degrees are presented in Table 1.

Table 1. Characteristics of the selected PEO-PPO-PEO copolymers and functionalization degrees of modified copolymers.

Chemical Formula [a]	**Pluronic F127**	**Pluronic P94**
	$PEO_{96}PPO_{56}PEO_{96}$	$PEO_{26}PPO_{48}PEO_{26}$
M_n (Da) [a]	11700	5000
M_n PEO blocks (Da) [a]	8500	2200
M_n PPO block (Da) [a]	3200	2800
CDI activation efficiency [a]	86%	67%
NH_2 modification efficiency [a]	91%	82%
p-SCN-Bn-DTPA conjugation efficiency [b]	82%	81%

[a] Determined by ^{1}H-NMR

[b] Determined by TLC and gamma-counter

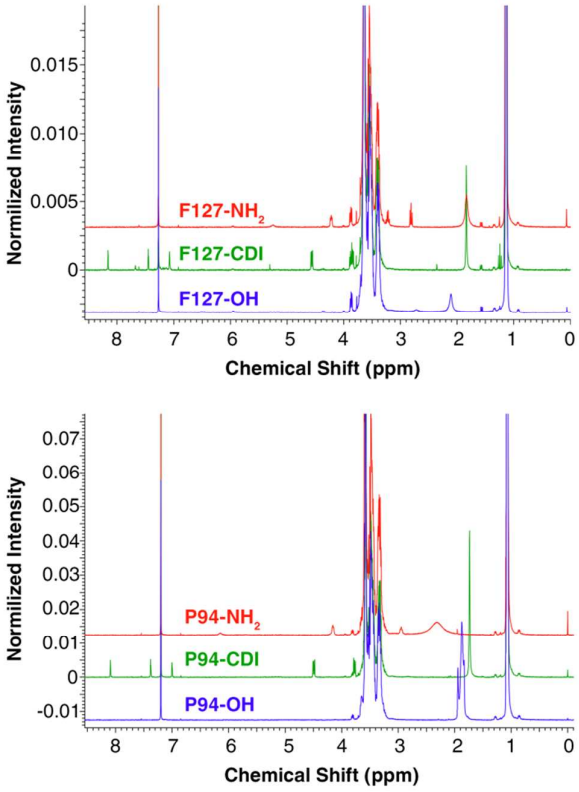

Figure 1. ^{1}H-NMR spectrums of Pluronic copolymers and intermediate synthesis products.

Physicochemical characterization of Pluronic nanocarriers

Pluronic triblock copolymers in their molecular form (unimers) and supramolecular assemblies (cross-linked micelles) with different PEO block length were used (Figure 2). The hydrodynamic size of the nanocarriers was determined below their cmT (15°C) (Table 2). The unimers are expected to be highly compact possibly with the PEO blocks forming a tight shell around the non-hydrated PPO block.[18] Due to the larger length of the PEO block, Pluronic F127 unimers exhibits a slightly larger hydrodynamic diameter than Pluronic P94 unimers.

To avoid the disassembly of Pluronic micelles *in vivo*,[6] their spherical structure was stabilized by UV-polymerization of pentaerythrol tetraacrylate (PETA) in the micellar core at 60ºC.[5] Stabilized Polymeric Micelles (SPM) of Pluronic P94 and F127 (SPM-P94 and SPM-F127 respectively) were then obtained. Light scattering characterization confirmed they were monodisperse systems that do not disassemble below the cmT (15ºC), and present an average hydrodynamic diameter of 30-35 nm and a slightly negative zeta potential (Table 2). Moreover, the size of the cross-linked carriers did not vary significantly at higher temperatures (Table S1).

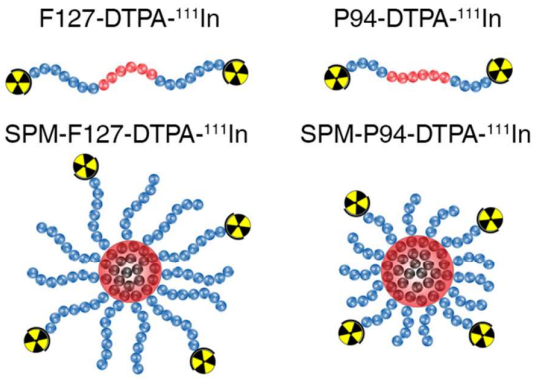

Figure 2. Molecular (F127-DTPA-^{111}In and P94-DTPA-^{111}In) and supramolecular (SPM-F127-DTPA-^{111}In and SPM-P94-DTPA-^{111}In) Pluronic nanocarriers investigated *in vivo*.

Table 2. Hydrodynamic diameter (D_H) and zeta potential (ζ) of Pluronic unimers (F127 and P94) and Stabilized Polymeric Micelles (SPM-F127 and SPM-P94).

Compound	**$D_{H,\ 15\ °C}$ (nm)**	**ζ (mV)**
F127	5.8 ± 0.4	Neutral[a]
SPM-F127	32.4 ± 2.4	- 13.3 ± 1.3
P94	4.2 ± 0.4	Neutral[a]
SPM-P94	29.2 ± 1.0	- 9.9 ± 0.3

[a] Not measurable by equipment

Radiolabeling efficiency and purity

Radiolabeling of nanocarriers was performed under standard labelling conditions for DTPA and ^{111}In (PBS and room temperature). The radiolabeling efficiencies were determined by TLC coupled to gamma-scintillation and are presented in Table 3. The DTPA modified copolymers (P94-DTPA and F127-DTPA) presented high labelling efficiencies (>95%), while radiolabeling of the stabilized micelles (SPM-F127-DTPA and SPM-P94-DTPA) was less efficient (~50%). Purification by size exclusion chromatography of the supramolecular carriers allowed us to obtain efficiencies of nearly 100%, which was suitable to perform *in vivo* SPECT studies.

Table 3. Radiolabeling efficiencies of DTPA-modified Pluronic nanocarriers.

Compound	^{111}In labelling efficiency[a]	^{111}In labelling efficiency[a] after purification
F127-DTPA-^{111}In	95%	[b]
SPM-F127-DTPA-^{111}In	45%	99%[c]
P94-DTPA-^{111}In	99%	[b]
SPM-P94-DTPA-^{111}In	53%	97%[c]

[a] Determined by TLC and gamma-counter

[b] No purification needed

[c] Purification with Sephadex G25 column

Radiolabeling stability of ^{111}In in mouse serum and PBS

The stability of the DTPA-^{111}In complex in all the nanocarriers was evaluated at 37ºC in both mouse serum (Figure 3A) and PBS (Figure 3B). The comparison between the two solvents allowed to assess the role of chelating proteins present in the serum (e.g. transferrin) on the stability of the DTPA-^{111}In complexes. The stability was quantified by TLC and gamma-scintillation.

After 72h, the loss of ^{111}In remained low: about 5-7% for F127-DTPA-^{111}In, SPM-F127-DTPA-^{111}In and P94-DTPA-^{111}In. However, the cross-linked micelles with the shorter PEO corona (SPM-P94-DTPA) were less stable revealing a 24% ^{111}In loss after 2h in the presence of mouse serum. Complex instability was also observed in PBS but at a slower rate.

It is known that complexes of DTPA-^{111}In present some *in vivo* instability and can dissociate at a rate of 5-9% loss per day for low molecular weight compounds,[19-21] and up to 20% loss in 24h for e.g. polymersomes with the DTPA-^{111}In complexes on their surface.[22] In comparison, the present nanocarriers displayed a better overall labelling stability, without significant ^{111}In loss in the presence. Only SPM-P94-DTPA-^{111}In showed both higher ^{111}In loss and sensitivity to the medium. The fact that the loss of ^{111}In with SPM-P94-DTPA seemed to stabilize after a few hours in the serum suggests that only a finite fraction of the complexes formed at the

surface are weakly bound. In the case of PBS medium, there is no competition with proteins and the dissociation kinetics are much slower, i.e. the 25% of ^{111}In loss observed for SPM-P94-DTPA-^{111}In in the serum is not reached after 3 days in PBS buffer.

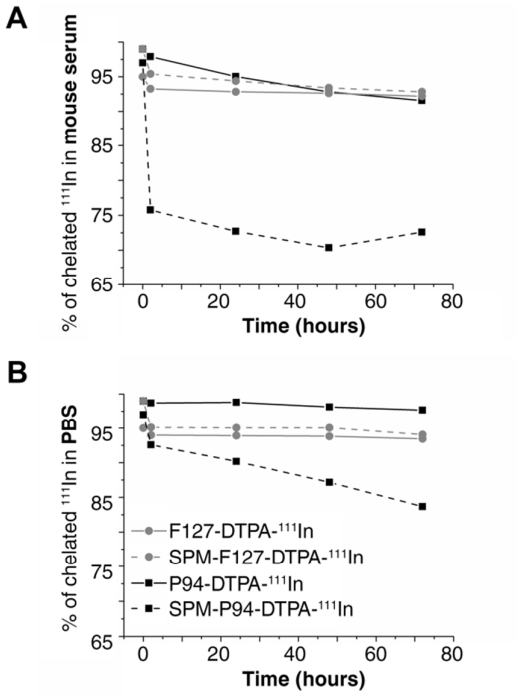

Figure 3. *In vitro* stability of ^{111}In radiolabeled Pluronic nanocarriers at 37^{o}C after dilution in (A) mouse serum and in (B) PBS for 72h.

SPECT imaging of Pluronic nanocarriers

Figures 4 shows top view maximum intensity projections (MIPs) on total body SPECT/CT scans at various time points after administration of ^{111}In-labeled Pluronic nanocarriers, illustrating dynamic changes in compounds' distribution over imaging days. For better visualization, the activity in the bladder in 0h p.i. scans was manually cropped from the SPECT images. Animated images of rotating MIPs can be visualized in the supplementary information (Videos S1-S4). The total activity remaining in the animal body (%ID) and the

specific uptake in the main organs (liver, spleen, heart, kidney, lungs and brain) (%ID/mL) for all imaging time-points are summarized in Figure 4, Table 4 and Table S2.

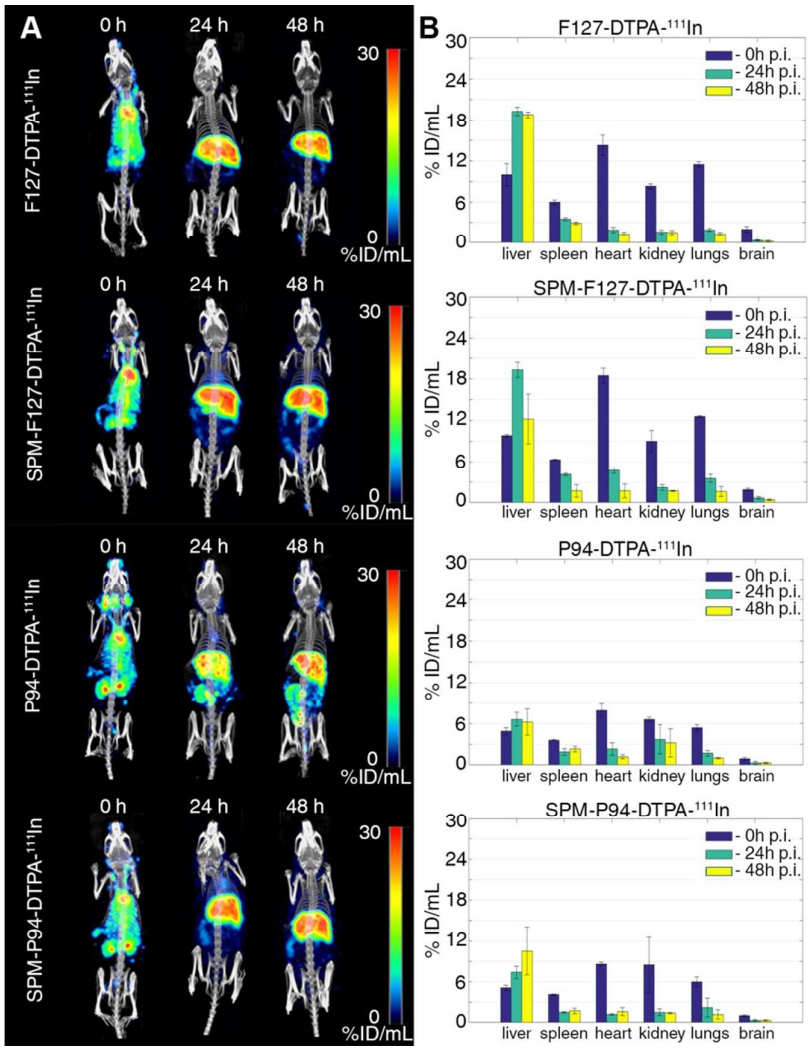

Figure 4. (A) Maximum intensity projections of total body SPECT/CT scans, acquired at 0, 24 and 48 hours post injection of ^{111}In-radiolabeled nanocarriers. (B) Quantified uptake of the carriers in selected organs of interest.

Table 4. Total body activity retention of Pluronic nanocarriers in the body of the animal 0, 24 and 48h post-injection (p.i.) time points, measured from the total body SPECT scans and expressed as % of the initially injected dose (ID).

Compound	Total body retention in % ID		
	0h p.i./SPECT	24 h p.i./SPECT	48 h p.i./SPECT
F127-DTPA-^{111}In	81.2[a]±3.6[b]	69.3±3.5	63.8±3.0
SPM-F127-DTPA-^{111}In	80.7±0.4	70.4±1.9	61.4±1.2
P94-DTPA-^{111}In	67.5±3.21	44.9±1.3	40.2±0.6
SPM-P94-DTPA-^{111}In	61.9±3.3	31.6±3.1	31.1±3.0

[a] Value does not include ^{111}In activity in the bladder of the animal

[b] Standard deviation within one study group of the animals

Our results show that all compounds have an initial renal clearance, which is higher for the P94-based carriers (~35% for P94 and ~19% for F127 compounds) (Table 4). At the same time, none of the carriers was accumulated in the skeleton (Figure 4A), what indicates minimal dissociation of ^{111}In in its ionic form the carriers after i.v. administration.[23, 24]

Analyses of the late stage biodistribution (24 and 48h p.i.) indicate that clearance of the nanocarriers occurs mainly through the liver. High uptake in this organ was associated with a higher PEO block length (F127-DTPA-^{111}In and SPM-F127-DTPA-^{111}In) (Figure 4, Table S2). Statistical analysis of the organs uptake showed that only the uptake in the liver and spleen was influenced by the PEO block length and aggregation state of the carriers. Tissue accumulation in the liver strongly correlated between unimers P94 and F127 ($R>0.98$) and remained independent for other compounds. The retention in the liver at 48h was also influenced by the aggregation state of the copolymers. In particular, SPM-P94-DTPA-^{111}In were more retained (10.5±3.5 %ID/mL) than the respective P94 unimers (6.2±1.9 %ID/mL), while SPM-F127-DTPA-^{111}In were more efficiently excreted (12.2±3.6 %ID/mL) than the corresponding F127 unimers (18.8±0.4 %ID/mL) (Figure 4, Table S2).

In the case of spleen uptake, statistical analysis revealed that only the stabilized micelles of the different Pluronics had uncorrelated tissue decomposition of ^{111}In-labeled compound. Aspects of liver and hepatobiliary uptake of the compounds were further investigated through the abdominal area of the animals (Figure 5 and Supplementary Figures S2-S5). Images show remaining spleen and intestinal uptake and generally high uniform liver uptake for all compounds. In the case of P94 unimers, the liver distribution is less uniform and we observed spreading of the radioactivity into the surrounding intestinal tissues (Figure 5).

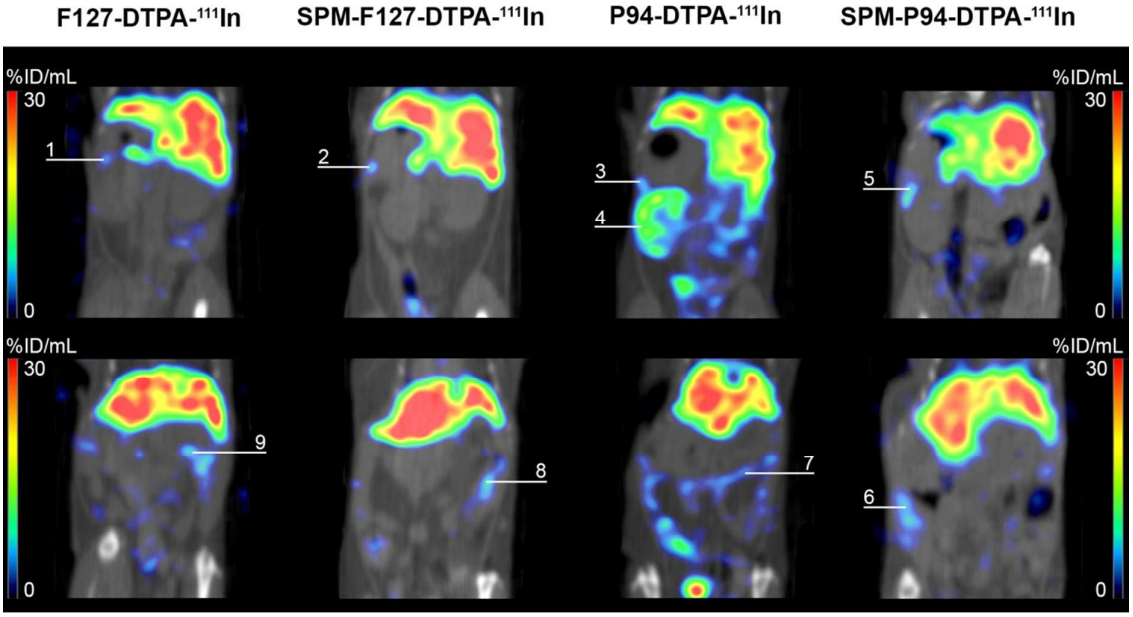

Figure 5. Abdominal area slices from the 48 hours post-injection total body SPECT/CT scans of mice injected with Pluronic nanocarriers. Images illustrate uptake in the spleen (1-3,5) and the intestines (6-9) for all compounds tested. At the same time, only P94-DTPA-^{111}In showed minor trapping of the compound in the renal cortex of the animal (4).

Although Pluronic F127 is approved by the FDA for i.v. use in humans, its initial biodistribution has never been evaluated *in vivo*. To get insight on the early stage uptake dynamics, we performed a dynamic scan with F127-DTPA-^{111}In. The video of the dynamic SPECT scan is available in the Supplementary Video 5, and the corresponding TACs are

presented in Figure 6. The uptake in main organs (heart, kidneys, liver, lungs and spleen) was almost immediate and distribution is achieved about 1 min after injection. The renal clearance started 1 min p.i., after which activity in the bladder gradually increased during the scan. The circulation of the compound in the systemic circulation was also clear throughout the scan due to high activity in the heart and arteries (see Video S5). Particularly in the lungs, the %ID/mL decreased from 25% to 11.5% in 30 min (Figure 6, Table S2). This high activity observed immediately after injection is associated with the high perfusion of this organ (8 mL/min) over the lower blood flow in other organs such as liver (1.8 mL/min), spleen (0.09 mL/min) and kidneys (1.3 mL/min).[25]

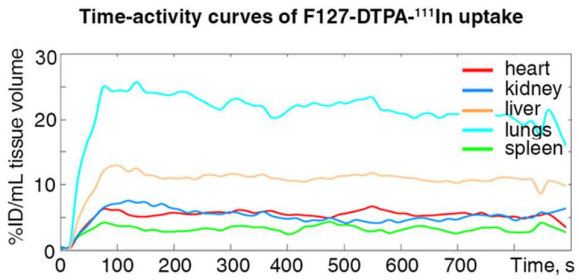

Figure 6. Time-activity curves of F127-DTPA-^{111}In shows %ID/mL uptake values for selected organs of interest in the mouse during first 15 min after the activity injection.

DISCUSSION

After functionalization of the nanocarriers with the chelator DTPA and evaluation of the radiolabeling efficiency and stability, we studied their biodistribution as a function of PEO block length and aggregation state (unimers versus stabilized micelles). Samples were administered below the cmc, i.e. the final concentration in the blood pool was ≤0.025% to assure comparison of molecular and supramolecular nanocarriers.

For the nanocarriers investigated in this work, a fraction of the radiolabeled compounds was rapidly excreted into the bladder after i.v. administration (Table 4). It is known that polymeric micelles and small nanoparticles with DTPA-^{111}In chelators can follow rapid loss of ^{111}In

and/or DTPA-^{111}In complexes after i.v. administration.[19-22] In the first case, ^{111}In in the form of free ions will rapidly bind to blood protein transferrin[23, 24] which will result in rapid accumulation and long retention of indium in the bone marrow and the liver,[26, 27] accompanied by relatively low clearance via renal filtration. Therefore, the observed initial renal clearance in our work is not related to dissociation of ^{111}In ions from the carriers. In the second case, the dissociation of DTPA-^{111}In complexes will result in rapid excretion of the activity into the urine (biological half-life ~ 1 hour, 95% ID excretion within 48h).[28, 29] Relatively high and prolonged activity retention in the body of the animals (Table 4) indicates that dissociation of ^{111}In-DTPA complexes from the carries should play only a minor role in the initial renal clearance of carriers studied in this work.

Although both Pluronic unimers are below the renal clearance threshold (30 kDa for linear PEG),[30] their renal filtration rates indicate molecular weight dependency, with nearly 20%ID of Pluronic F127 (12 kDa) and 30%ID of Pluronic P94 (5 kDa) eliminated 30 min p.i.. The stabilized micelles (SPM-F127-DTPA-^{111}In and SPM-P94-DTPA-^{111}In) also presented initial renal clearance, which was faster for the SPM-P94-DTPA-^{111}In. Considering the low bone uptake for all compounds studied, the fast clearance of SPM-P94-DTPA-^{111}In (Table 4) should be predominantly attributed to the lower stability of the DTPA-^{111}In complexes in the presence of serum proteins (Figure 3A).

Overall, the organ with the highest uptake of the radioactive compounds was the liver (Figure 4, Table S2). This accumulation mainly occurs through internalization by the hepatocytes and the Kupffer cells.[25] The passage of the nanocarriers through the liver endothelial fenestrations leads to their metabolisation by the hepatocytes and elimination into the bile and intestinal tract. We have observed at late time points (24 and 48h) activity in the intestines for all compounds (Figure 5), showing that the nanocarriers were excreted via the hepatobiliary system. Late time-points SPECT of P94 unimers showed spreading of the compound into the

surrounding tissues of the gastrointestinal tract (Figure 5), which can be explained by their small size (Table 2) and diffusion through endothelial junctions. The uptake by Kupffer cells occurs as a result from opsonization by serum proteins in the systemic circulation. To avoid opsonization, the surface of the nanomaterials can be modulated using PEO, which also depends on the chain length and PEO surface density.[31]. Corona chains in Pluronic micelles have a "mushroom" conformation[32] associated with a lower density of PEO chains and larger fluctuations of the local PEO concentration, which can facilitate the adsorption of plasma proteins onto the hydrophobic core. Pluronic micelles can then be recognized by the Kupffer cells. The two-fold increase in the liver uptake at 24h for the F127, SPM-F127 and SPM-P94 (Table S2) shows that clearance by the liver was delayed. In the case of P94 unimers, the uptake in the liver did not increase significantly during the 48 hours suggesting that the elimination of P94 unimers occurs mainly through renal filtration. In fact, the accumulation of P94-DTPA-^{111}In in the kidney was consistently higher (Figure 4, Table S2). In conclusion, we observed that the PEO block length affects the renal clearance and initial liver uptake of the compounds, whereas the aggregation state influences the retention in the liver at late-stages (48h).

The spleen uptake of all nanocarriers studied was low and decreased overtime indicating circulation without retention in the spleen sinusoidal sieve (Figure 4, Table S2). Nanocarriers with high rigidity, elongated or irregular shapes and/or large size (>70-90 nm) present generally high retention in the spleen.[22, 25] The ability of our nanocarriers to surpass the spleen clearance mechanisms suggests that they should achieve good biocompatibility and should not trigger immunogenic reactions.

None of the carriers studied were retained in the lungs (Table S2) due to their small size and flexibility.[25] Since Pluronics are not biodegradable,[7] the observed elimination pathways (renal and hepatic clearance) contribute to the biocompatibility of these systems.

CONCLUSIONS

We developed a new strategy to compare the biodistribution of Pluronic-based nanocarriers with different PEO block length and aggregation state. This approach eliminates the recurrent limitation associated with the dynamic nature of copolymer micelles and allows us to use similar concentrations of both types of nanocarriers.

Our results show that varying the PEO block length and aggregation state of the copolymers (unimers versus micelles), different renal and liver clearances are obtained. Outcomes of this work can be beneficial for a more rational development of Pluronic-based nanocarriers and for the future of EPR-based cancer therapies.

Acknowledgements: The research leading to these results has received funding from the People Programme (Marie Curie Actions) of the European Union's Seventh Framework Programme (FP7/2007-2013) under REA grant agreement no. PITN-GA-2012-317019 'TRACE 'n TREAT. F. J. Beekman is a founder, shareholder and CEO/CSO of MILabs.

Supporting Information Available:

Synthesis of DTPA-modified Pluronic unimers and radiolabeling with ^{111}In; FT-IR spectrum of raw, CDI-activated and amine-terminated copolymers; hydrodynamic diameter of Stabilized Polymeric Micelles at different solution temperatures; quantified uptake of Pluronic nanocarriers in multiple organs of the animals at 0, 24 and 48 hours p.i of the carriers; axial liver slices from focused late-stage abdominal SPECT scans of the animals; videos of rotating MIPs of total body SPECT/CT scans at 0, 24 and 48 hours p.i. of the radiolabeled compounds; SPECT-based video of 4D total body dynamics of F127-DTPA-^{111}In with corresponding quantified pharmacokinetics in organs of interest; and detailed information of the experimental section namely the materials used, commercial Pluronics

purification, CDI and amine-modification procedure, description of TLC systems used to determine DTPA conjugation efficiency and nanocarriers radiolabeling and DLS equipment. This material is available free of charge *via* the Internet at http://pubs.acs.org.

References

1. Duncan, R.; Gaspar, R. Nanomedicine(s) under the microscope. *Mol Pharm* **2011,** *8*, (6), 2101-2141.
2. Lammers, T.; Hennink, W. E.; Storm, G. Tumour-targeted nanomedicines: principles and practice. *Br J Cancer* **2008,** *99*, (3), 392-397.
3. Duan, X.; Li, Y. Physicochemical characteristics of nanoparticles affect circulation, biodistribution, cellular internalization, and trafficking. *Small* **2013,** *9*, (9-10), 1521-1532.
4. Krasia-Christoforou, T.; Georgiou, T. K. Polymeric theranostics: using polymer-based systems for simultaneous imaging and therapy. *J Mater Chem B* **2013,** *1*, (24), 3002-3025.
5. Arranja, A.; Schroder, A.; Schmutz, M.; Waton, G.; Schosseler, F.; Mendes, E. Cytotoxicity and internalization of Pluronic micelles stabilized by core cross-linking. *J Control Release* **2014,** *13*, 87-95.
6. Talelli, M.; Rijcken, C. J. F.; Hennink, W. E.; Lammers, T. Polymeric micelles for cancer therapy: 3 C's to enhance efficacy. *Curr Opin Solid State Mater Sci* **2012,** *16*, (6), 302-309.
7. Grindel, J. M.; Jaworski, T.; Piraner, O.; Emanuele, R. M.; Balasubramanian, M. Distribution, metabolism, and excretion of a novel surface-active agent, purified poloxamer 188, in rats, dogs, and humans. *J Pharm Sci* **2002,** *91*, (9), 1936-1947.
8. Willcox, M. L.; Newman, M. M.; Paton, B. C. A study of labeled pluronic F-68 after intravenous injection into the dog. *J Surg Res* **1978,** *25*, (4), 349-356.
9. Batrakova, E. V.; Li, S.; Li, Y.; Alakhov, V. Y.; Elmquist, W. F.; Kabanov, A. V. Distribution kinetics of a micelle-forming block copolymer Pluronic P85. *J Control Release* **2004,** *100*, (3), 389-397.
10. Wang, Z. Y.; Stern, I. J. Disposition in rats of a polyoxypropylene-polyoxyethylene copolymer used in plasma fractionation. *Drug Metab Dispos* **1975,** *3*, (6), 536-542.
11. Lu, H. F.; Lim, W. S.; Wang, J.; Tang, Z. Q.; Zhang, P. C.; Leong, K. W.; Chia, S. M.; Yu, H.; Mao, H. Q. Galactosylated PVDF membrane promotes hepatocyte attachment and functional maintenance. *Biomaterials* **2003,** *24*, (27), 4893-903.
12. Hoang, B.; Lee, H.; Reilly, R. M.; Allen, C. Noninvasive Monitoring of the Fate of 111In-Labeled Block Copolymer Micelles by High Resolution and High Sensitivity MicroSPECT/CT Imaging. *Mol Pharm* **2009,** *6*, (2), 581-592.
13. Ivashchenko, O.; van der Have, F.; Goorden, M. C.; Ramakers, R. M.; Beekman, F. J. Ultra-high-sensitivity submillimeter mouse SPECT. *J Nucl Med* **2015,** *56*, (3), 470-475.
14. Branderhorst, W.; Vastenhouw, B.; Beekman, F. J. Pixel-based subsets for rapid multi-pinhole SPECT reconstruction. *Phys Med Biol* **2010,** *55*, (7), 2023-2034.
15. van der Have, F.; Vastenhouw, B.; Rentmeester, M.; Beekman, F. J. System calibration and statistical image reconstruction for ultra-high resolution stationary pinhole SPECT. *IEEE Trans Med Imaging* **2008,** *27*, (7), 960-971.
16. King, M. A.; Glick, S. J.; Hendrik Pretorius, P.; Glenn Wells, R.; Gifford, H. C.; Narayanan, M. V.; Farncombe, T., Attenuation, Scatter, and Spatial Resolution Compensation in SPECT. In *Emission Tomography*, Aarsvold, M. N. W. N., Ed. Academic Press: San Diego, 2004; pp 473-498.
17. Wu, C.; de Jong, J. R.; Gratama van Andel, H. A.; van der Have, F.; Vastenhouw, B.; Laverman, P.; Boerman, O. C.; Dierckx, R. A.; Beekman, F. J. Quantitative multi-pinhole small-animal SPECT: uniform versus non-uniform Chang attenuation correction. *Phys Med Biol* **2011,** *56*, (18), N183-193.

18. Alexandridis, P.; Alan Hatton, T. Poly(ethylene oxide)-poly(propylene oxide)-poly(ethylene oxide) block copolymer surfactants in aqueous solutions and at interfaces: thermodynamics, structure, dynamics, and modeling. *Colloids Surf A Physicochem Eng Asp* **1995,** *96*, (1–2), 1-46.
19. Lub-de Hooge, M. N.; Kosterink, J. G. W.; Perik, P. J.; Nijnuis, H.; Tran, L.; Bart, J.; Suurmeijer, A. J. H.; de Jong, S.; Jager, P. L.; de Vries, E. G. E. Preclinical characterisation of (111)In-DTPA-trastuzumab. *Br J Pharmacol* **2004,** *143*, (1), 99-106.
20. Hnatowich, D. J. Label stability in serum of four radionuclides on DTPA-coupled antibodies—An evaluation. *Int J Rad Appl Instrum B* **1986,** *13*, (4), 353-358.
21. Patil, R. R.; Yu, J.; Banerjee, S. R.; Ren, Y.; Leong, D.; Jiang, X.; Pomper, M.; Tsui, B.; Kraitchman, D. L.; Mao, H.-Q. Probing In Vivo Trafficking of Polymer/DNA Micellar Nanoparticles Using SPECT/CT Imaging. *Mol Ther* **2011,** *19*, (9), 1626-1635.
22. Brinkhuis, R. P.; Stojanov, K.; Laverman, P.; Eilander, J.; Zuhorn, I. S.; Rutjes, F. P.; van Hest, J. C. Size dependent biodistribution and SPECT imaging of (111)In-labeled polymersomes. *Bioconjug Chem* **2012,** *23*, (5), 958-65.
23. Hosain, F.; McIntyre, P. A.; Poulose, K.; Stern, H. S.; Wagner, H. N., Jr. Binding of trace amounts of ionic indium-113m to plasma transferrin. *Clin Chim Acta* **1969,** *24*, (1), 69-75.
24. Adatepe, M. H.; Penkoske, P.; van Amberg, A.; Wharton, T.; Evens, R. G.; Potchen, E. J. Red cell and plasma protein labeling with 113mIn. *Int J Appl Radiat Is* **1971,** *22*, (8), 498-501.
25. Bertrand, N.; Leroux, J. C. The journey of a drug-carrier in the body: an anatomo-physiological perspective. *J Control Release* **2012,** *161*, (2), 152-163.
26. Kreyling, W. G.; Abdelmonem, A. M.; Ali, Z.; Alves, F.; Geiser, M.; Haberl, N.; Hartmann, R.; Hirn, S.; de Aberasturi, D. J.; Kantner, K.; Khadem-Saba, G.; Montenegro, J.-M.; Rejman, J.; Rojo, T.; de Larramendi, I. R.; Ufartes, R.; Wenk, A.; Parak, W. J. In vivo integrity of polymer-coated gold nanoparticles. *Nat Nano* **2015,** *10*, (7), 619-623.
27. Ohtake, Y.; Maruko, A.; Satoh, S.; Ohkubo, Y. The uptake of 111In in the liver and bone marrow of partially hepatectomized and venesectioned rats. *Appl Radiat Isot* **2008,** *66*, (9), 1245-1249.
28. Harrington, K. J.; Rowlinson-Busza, G.; Syrigos, K. N.; Uster, P. S.; Abra, R. M.; Stewart, J. S. Biodistribution and pharmacokinetics of 111In-DTPA-labelled pegylated liposomes in a human tumour xenograft model: implications for novel targeting strategies. *Br J Cancer* **2000,** *83*, (2), 232-8.
29. Matsushima, H.; Kato, M.; Sugimura, Y.; Hazue, M. In vivo behavior of 111In-DTPA in rat and mouse after intra-ventricular administration. *Radioisotopes* **1977,** *26*, (11), 784-9.
30. Yamaoka, T.; Tabata, Y.; Ikada, Y. Distribution and tissue uptake of poly(ethylene glycol) with different molecular weights after intravenous administration to mice. *J Pharm Sci* **1994,** *83*, (4), 601-606.
31. Klibanov, A. L.; Maruyama, K.; Torchilin, V. P.; Huang, L. Amphipathic polyethyleneglycols effectively prolong the circulation time of liposomes. *FEBS Lett* **1990,** *268*, (1), 235-237.
32. Bhattacharjee, J.; Verma, G.; Aswal, V. K.; Patravale, V.; Hassan, P. A. Microstructure, drug binding and cytotoxicity of Pluronic P123-aerosol OT mixed micelles. *RSC Adv* **2013,** *3*, (45), 23080-23089.

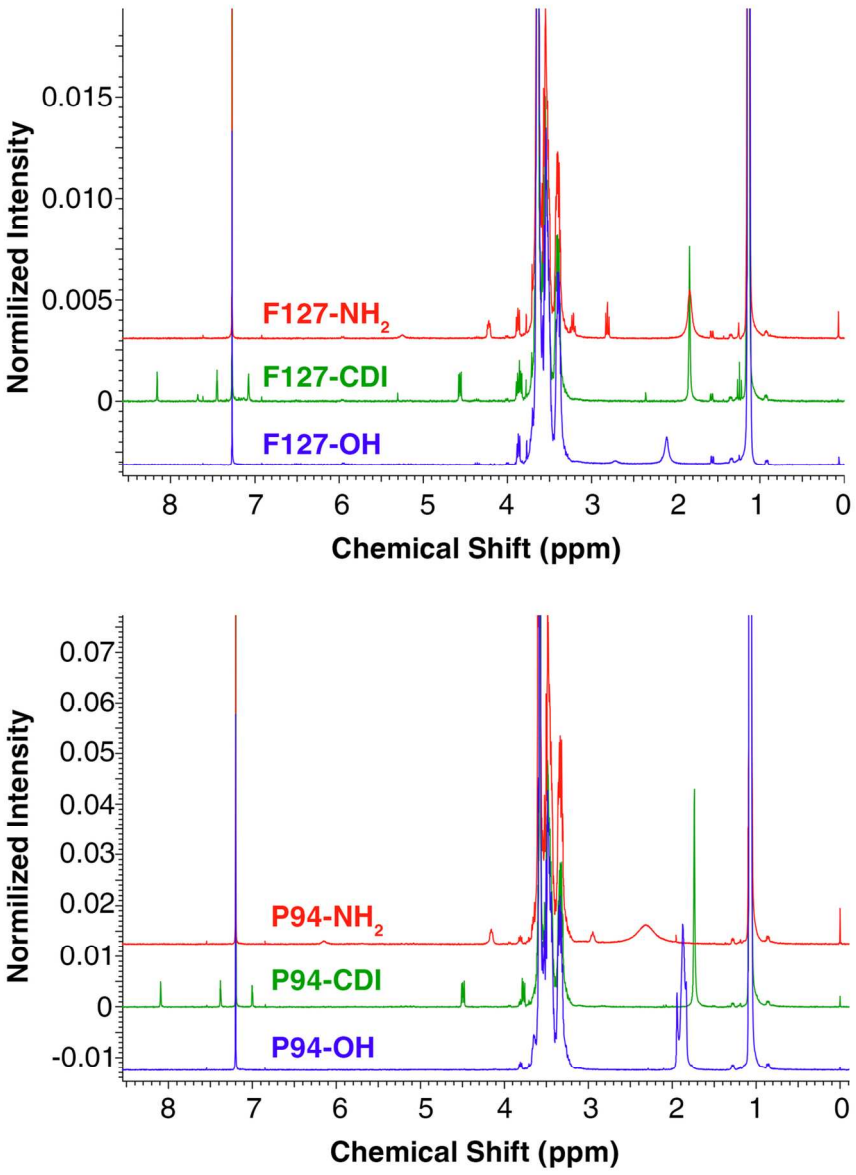

Figure 1. ^{1}H-NMR spectrums of Pluronic copolymers and intermediate synthesis products.
113x156mm (300 x 300 DPI)

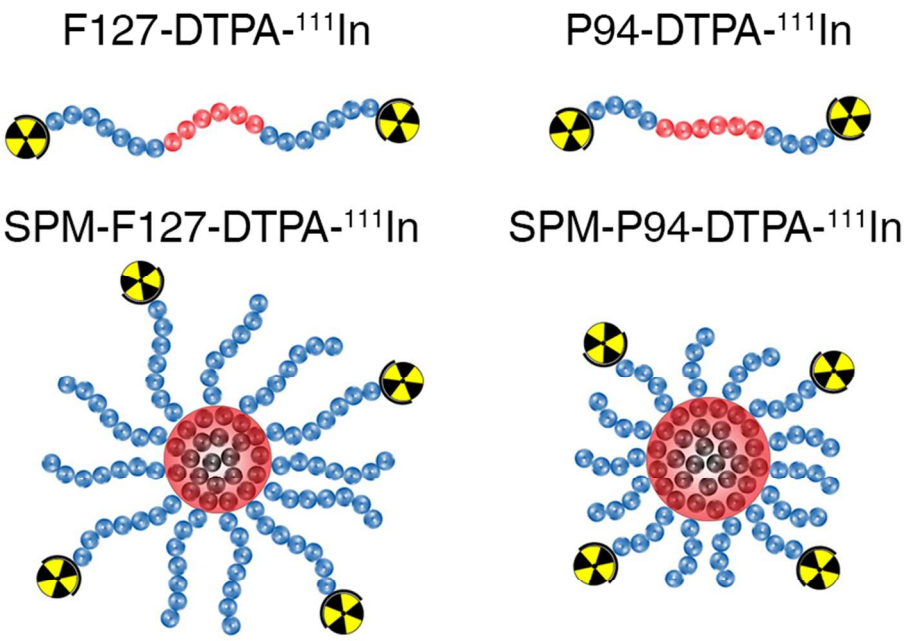

Figure 2. Molecular (F127-DTPA-^{111}In and P94-DTPA-^{111}In) and supramolecular (SPM-F127-DTPA-^{111}In and SPM-P94-DTPA-^{111}In) Pluronic nanocarriers investigated *in vivo*.
82x58mm (300 x 300 DPI)

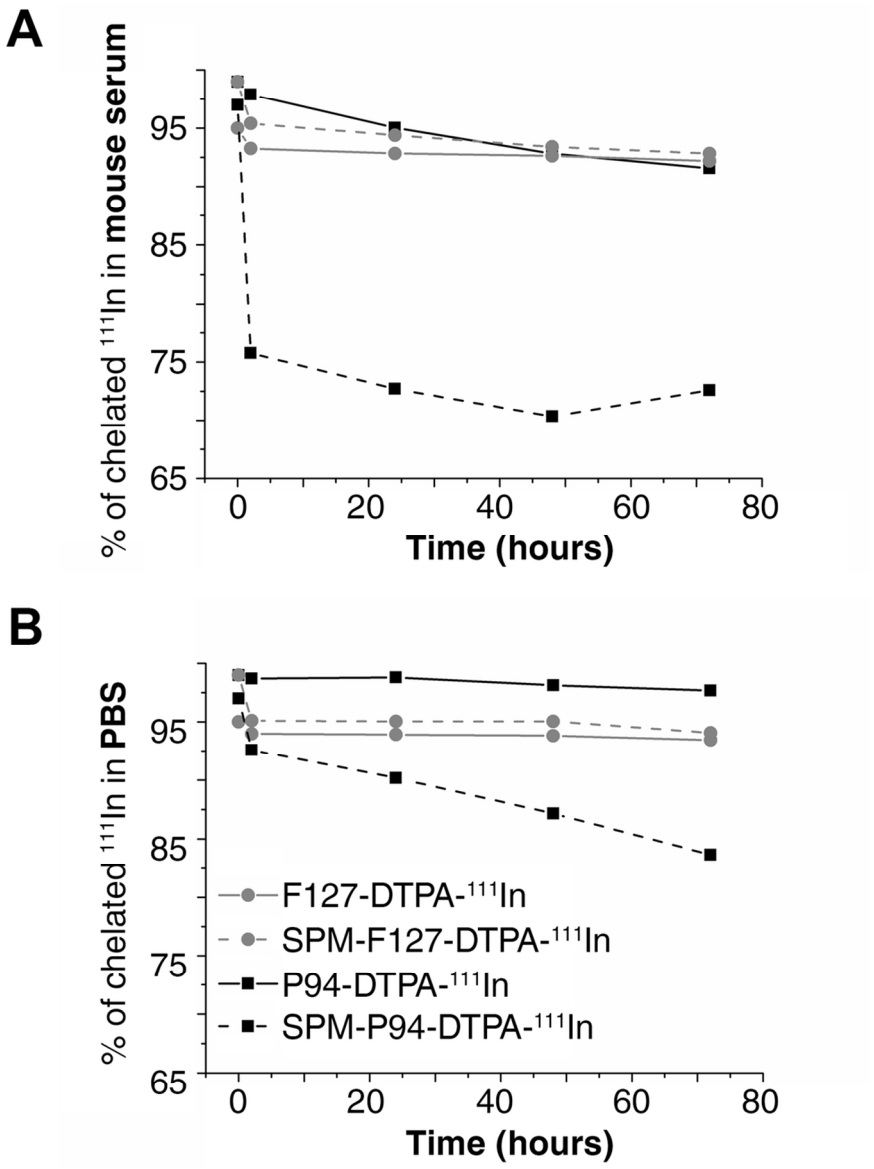

Figure 3. *In vitro* stability of ^{111}In radiolabeled Pluronic nanocarriers at 37°C after dilution in (A) mouse serum and in (B) PBS for 72h.
99x133mm (300 x 300 DPI)

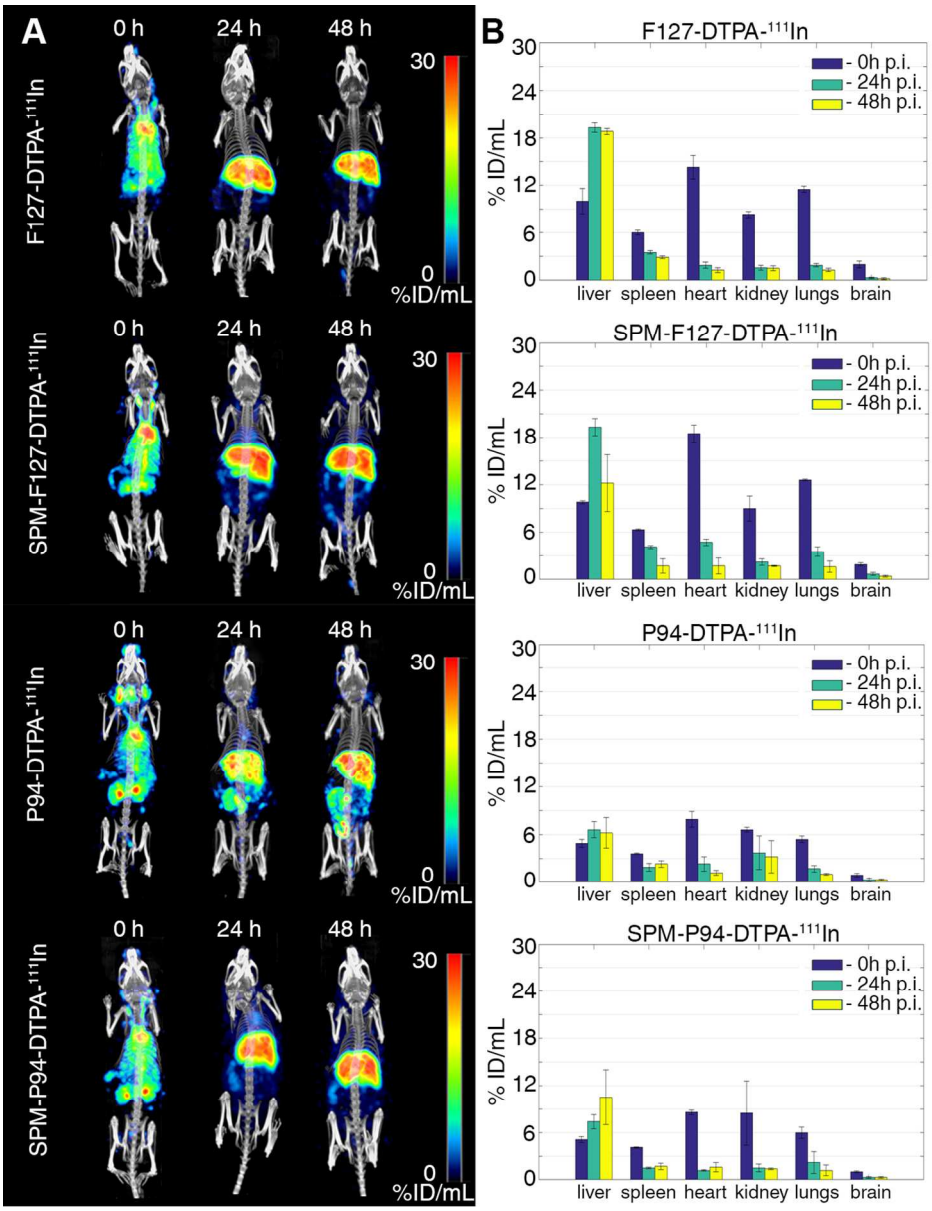

Figure 4. (A) Maximum intensity projections of total body SPECT/CT scans, acquired at 0, 24 and 48 hours post injection of ^{111}In-radiolabeled nanocarriers. (B) Quantified uptake of the carriers in selected organs of interest.
113x146mm (300 x 300 DPI)

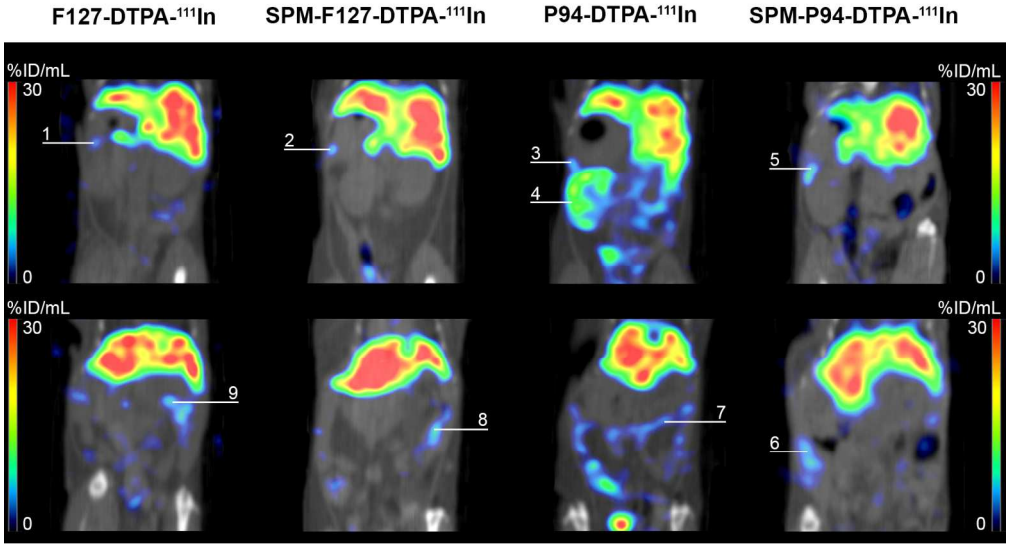

Figure 6. Time-activity curves of F127-DTPA-^{111}In shows %ID/mL uptake values for selected organs of interest in the mouse during first 15 min after the activity injection.
158x87mm (300 x 300 DPI)

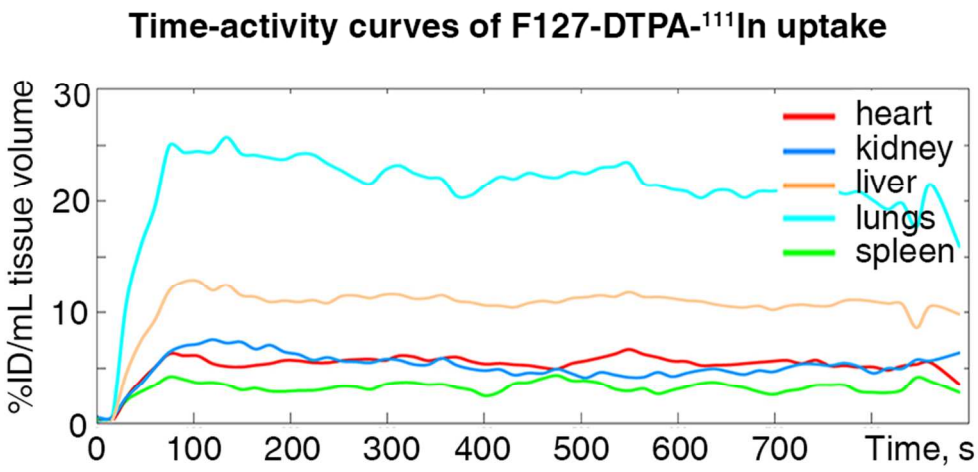

Figure 6. Time-activity curves of F127-DTPA-^{111}In shows %ID/mL uptake values for selected organs of interest in the mouse during first 15 min after the activity injection.
82x41mm (300 x 300 DPI)